Super synergy between photocatalysis and ozonation using bulk g-C$_3$N$_4$ as catalyst: A potential sunlight/O$_3$/g-C$_3$N$_4$ method for efficient water decontamination

Jiadong Xiao [a,b], Yongbing Xie [a,*], Faheem Nawaz [a,b], Song Jin [a], Feng Duan [a,b], Mingjie Li [a], Hongbin Cao [a,c,**]

[a] National Engineering Laboratory for Hydrometallurgical Cleaner Production Technology, Beijing Engineering Research Center of Process Pollution Control, Key Laboratory of Green Process and Engineering, Institute of Process Engineering, Chinese Academy of Sciences, Beijing 100190, China
[b] University of Chinese Academy of Sciences, Beijing 100049, China
[c] Collaborative Innovation Center of Chemical Science and Engineering (Tianjin), Tianjin 300072, China

ARTICLE INFO

ABSTRACT

The recent thrust in utilizing g-C$_3$N$_4$ as a metal-free photocatalyst has led to accelerated attention in environmental decontamination. Despite of enormous efforts paid on material modification, the overall efficiency is still limited, especially for decomposition of chemically stable contaminants and mineralization of organics. Here, we coupled bulk g-C$_3$N$_4$ (GCN-T and GCN-D synthesized from thiourea and dicyandiamide, respectively) photocatalysis with ozonation for mineralization of oxalic acid (OA) and *p*-hydroxybenzoic acid (PHBA) under UV and visible-light irradiation. The compelling experiments confirmed that bulk g-C$_3$N$_4$ could trigger a super synergy between photocatalysis and ozonation under visible light. The apparent rate constant of OA removal by Vis/O$_3$/GCN-D was 20.6 times as great as the sum of that in Vis/GCN-D and ozonation. The TOC removal of PHBA by Vis/O$_3$/GCN-D was 98.0%, which was about 39.3% higher than the sum of that in Vis/GCN-D and ozonation. The high conduction band (CB) position of g-C$_3$N$_4$ proved to be crucial for the synergy between photocatalysis and ozonation. GCN-D possessed a ∼0.10 V upshifted CB level compared to GCN-T, resulting in a 1.30 times higher photocatalytic ozonation activity. More negative CB potential benefited photoinduced electron capture by ozone molecules, thus significantly enhanced charge separation as well as the decay of ozone eventually with generation of abundant hydroxyl radicals (•OH). Exceptionally, Vis/O$_3$/GCN-D exhibited stronger oxidizing ability than UV/O$_3$/GCN-D for OA degradation with the same light intensity. The reason was that the photolysis of ozone occurred under UV and partly inhibited ozone capturing photoinduced electrons. The amount of generated •OH thus decreased in UV/O$_3$/GCN-D instead with the formation of a few atomic oxygen species (O (^{1}D)). This study puts forward new application of the easily obtained bulk g-C$_3$N$_4$ and may drive the advance of sunlight/O$_3$/g-C$_3$N$_4$ method for efficient and green water decontamination using sunlight as energy source.

© 2015 Elsevier B.V. All rights reserved.

1. Introduction

Semiconductor-based photocatalysis has attracted worldwide attention due to its potential in environmental and energy-related applications. For the purpose of taking full advantage of solar energy, enormous efforts have been devoted to searching suitable materials with high visible-light response. Among various semiconductor materials, the recent thrust in utilizing graphitic carbon nitride (g-C$_3$N$_4$) as a metal-free photocatalyst has aroused accelerated concern in water decontamination [1–4]. Bulk g-C$_3$N$_4$ can be easily obtained through direct polymerization of cheap feedstocks and its narrow bandgap of 2.7 eV permits it to absorb visible light directly [5]. Additionally, g-C$_3$N$_4$ exhibits high thermal and chemical stability, owing to its tri-*s*-triazine ring structure and high degree of condensation [5]. Hence, g-C$_3$N$_4$ is considered to be a potential photocatalyst for practical application in water treatment on a large scale, and triggered the recent flood of interest.

Unfortunately, there exist two main drawbacks in terms of bulk g-C$_3$N$_4$ as an efficient photocatalyst. Firstly, the rapid recombination of photoinduced electron-hole couples could largely decrease the quantum yield of bulk g-C$_3$N$_4$. Secondly, the high valance band (VB) position seriously limits its catalytic activity. To solve these problems, the majority of research focuses on the modification of g-C$_3$N$_4$ such as building mesoporous structure [1,6], doping with metal or nonmetal elements [7–10] and coupling with other semiconductors [11,12] or conjugated polymers [13,14]. Despite of great efforts are paid, the overall photocatalytic efficiency is still limited, especially for decomposition of chemically stable contaminants.

It is well known that the combination of various advanced oxidation processes (AOPs) may lead to an enhanced production of oxidative species, and consequently accelerate the degradation and mineralization of refractory contaminants [15,16]. In this sense, the integration of g-C$_3$N$_4$ photocatalysis with ozonation can be a promising treatment method [15–17]. The conduction band (CB) of g-C$_3$N$_4$ is reported to be −1.3 V versus normal hydrogen electrode (NHE), which is quite more negative than that of TiO$_2$ (−0.5 V versus NHE) [2]. Meanwhile, ozone is a more powerful oxidant than oxygen, and it can quickly capture the strong reducing electrons upon CB of g-C$_3$N$_4$. This would promote the separation of photoinduced electron–hole couples, decomposition of ozone, and consequently generate more oxidative species. Very recently, two studies have announced that bulk g-C$_3$N$_4$ without any modification could trigger a super synergy between visible-light photocatalysis and ozoantion thereupon with dramatically enhanced oxidation efficiency [18,19]. However, a further investigation to identify the most significant property of the catalyst itself in terms of promoting photocatalytic ozonation activity is still requisite, which would advance the development of this environmentally friendly and energy-saving water treatment technology. It is also important to compare the coupling efficiency and mechanism under ultraviolet (UV) and visible-light irradiation, in order to assess the prospect of g-C$_3$N$_4$-mediated solar photocatalytic ozonation.

In this study, two kinds of bulk g-C$_3$N$_4$ (GCN-T and GCN-D) were synthesized using thiourea and dicyandiamide as the precursor, respectively. Their structural, optical and electrochemical properties and hence, the activities in catalytic ozonation, photocatalytic oxidation and photocatalytic ozonation processes were investigated detailedly. Oxalic acid (OA) was chosen as the targeted pollutant, as it is a recalcitrant intermediate in oxidation of many organic compounds, and is often used to characterize the efficiency of oxidation methods [20,21]. The mineralization of *p*-hydroxybenzoic acid (PHBA) was also adopted to evaluate the oxidizing ability of various processes. It was found that the upshifted CB position of g-C$_3$N$_4$ is the most significant for the enhanced photocatalytic ozonation efficiency. Moreover, Vis/O$_3$/g-C$_3$N$_4$ exhibited improved oxidation ability than UV/O$_3$/g-C$_3$N$_4$ with the same light intensity. The oxidation mechanism of these two processes was systematically studied, and two different generation pathways of the involved oxidative species were proposed correspondingly.

2. Experimental

2.1. Materials and reagents

Dicyandiamide, thiourea, OA and PHBA were purchased from Sinopharm Chemical Reagent Co., Ltd., China. *Tert*-butanol (tBA) and *p*-benzoquinone (pBQ) were supplied by Xilong Chemical Co., Ltd., China. Ultrapure oxygen gas (purity 99.999%) and nitrogen gas (purity 99.999%) were provided by Beijing Qianxi Gas Co., Ltd., China. All chemicals used in this study were at least in analytical grade without further purification. Ultra-pure water was used for all synthesis and treatment.

2.2. Catalyst preparation

GCN-T and GCN-D were obtained by direct polycondensation of dicyandiamide and thiourea, respectively. Typically, 15 g of dicyandiamide or thiourea was put in an alumina crucible, which was then transferred into a muffle furnace and heated to 550 °C for 2 h with a heating rate of 15 °C/min. The final products were collected, washed with ultrapure water and ethanol, and ground into powder for further use.

2.3. Catalyst characterization

The crystal phase was characterized by X-ray diffraction (XRD) (X'PERT-PRO MPD) with a Cu$_{K\alpha}$ irradiation (λ = 0.15406 nm). The morphologies and structures of the prepared samples were further investigated by field emission scanning electron microscopy (FESEM, JEOL JSM-6700F, Japan). The Brunauer–Emmett–Teller (BET) surface areas, total pore volumes and average pore sizes were measured by an automated gas sorption analyzer (Autosorb-iQ, Quantachrome, USA). Pore size distribution was calculated with the Non Localized Density Functional Theory method using the adsorption data. The UV–vis diffuse reflectance spectra (DRS) of the samples were obtained using Varian Cary 5000, USA. X-ray photoelectron spectroscopy (XPS) data were obtained on an ESCALAB 250Xi instrument (Thermo Fisher Scientific, USA). Electrochemical and photoelectrochemical measurements were performed in a three-electrode cell with 0.1 mol/L (M) Na$_2$SO$_4$ as the electrolyte solution using an electrochemical analyzer (Autolab PGSTAT302N, Metrohm, Switzerland). A 1 cm × 1 cm indium tin oxide (ITO) glass electrode and a standard calomel electrode (SCE) were used as the counter electrode and the reference electrode, respectively. The working electrode were prepared as follows: 1.5 mg of the as-prepared photocatalyst was mixed with 0.5 mL of isopropanol under sonication for 30 min to produce a slurry, which was then loaded and dip-coated onto a 1 cm × 1 cm ITO glass electrode. The electrode was then exposed to air atmosphere for 24 h to eliminate isopropanol for further test.

2.4. Photocatalytic ozonation experiments

The photocatalytic ozonation was carried out at 25 °C under UV (200–400 nm) or visible light (420–800 nm) in a 450 mL cylindrical borosilicate glass reactor with a quartz cap and a porous glass plate at the bottom, containing 300 mL solution with 1 mM of OA and 1 g/L of catalyst. Fig. S1 illustrates the experimental set-up. Typically, gaseous ozone was continuously bubbled through a porous plate into the reactor with a flow rate of 100 mL/min and an ozone concentration of 30 mg/L. Meanwhile, the solution was irradiated with an average radiant flux of 365 mW/cm^2. UV irradiation (200–400 nm) was provided by a 300 W Xenon lamp (CEL-NP2000, Aulight Co., Ltd., China) equipped with a UV reflector, while visible light (420–800 nm) was produced by the same lamp equipped with a visible-light reflector and a 420 nm cutoff filter. Ozone was generated from ultrapure oxygen by an ozone generator (Anseros COM-AD-01, Germany). Single photocatalysis and ozonation experiments were conducted using the same reactor. For photocatalytic degradation, during each run, the solution was magnetically stirring in dark for 30 min to obtain an adsorption–desorption equilibrium before reaction. The OA concentration was analyzed by high performance liquid chromatography (HPLC, Agilent series 1200, USA) equipped with a Zorbax SB-Aq column and a UV–Vis detector qualified at 210 nm.

The mobile phase was a mixture of methanol and water containing 10 mM H_3PO_4 (20/80%, v/v).

3. Results and discussion

3.1. Structural properties of as-prepared samples

The XRD patterns of GCN-T and GCN-D are presented in Fig. 1a. A typical graphitic stacking C_3N_4 structure was confirmed by two obvious peaks. The intensive diffraction peak at 27.5° was an inter-layer stacking peak of aromatic systems as indexed as the (0 0 2) plane, and the relatively weak peak at 13.1° labeled as (1 0 0) plane corresponded to the in-plain structural packing motif of tristri-azine units [3,22]. The peak intensity of GCN-D was stronger than that of GCN-T, indicating a higher condensation degree and higher crystallinity, which was in agreement with the reported litera-tures [23,24]. Fig. 1b shows the nitrogen adsorption–desorption isotherms and the corresponding pore size distribution for GCN-T and GCN-D, respectively. The isotherms of the two samples were close to type IV, which implied the presence of mesopores [23]. The pore size distribution curves further confirmed the formation of varisized mesopores in the two bulk materials. GCN-T had meso-pores of 4.0, 5.4, 6.2, 7.5, 10.7, 15.3 and 30.1 nm from the inlet of Fig. 1b. The aggregation of nanosheets and nanoparticles created many bumps and hollows, contributing to the generation of these mesopores (Fig. 2a). The GCN-D sample had larger pores of 9.3, 10.7, 16.0 and 30.1 nm, which could be ascribed to the impacted layer structure on a large scale (Fig. 2b). Correspondingly, the spe-cific surface area of GCN-T was 16.3 m^2/g, which was larger than 2.7 m^2/g for GCN-D (Table S1).

The morphologies of the prepared materials were further revealed by the FESEM images in Fig. 2. The GCN-D sample dis-played an impacted smooth layer structure with a large size (Fig. 2b), while GCN-T had coarse surfaces with a number of bumps and hollows, during which varisized mesopores were formed (Fig. 2a). It indicated GCN-T had a relatively larger sur-face area, which was in accordance with the pore size distribution results.

The XPS measurements were carried out to determine the chem-ical state of the elements for GCN-T and GCN-D, as shown in Fig. 3. Signals of C, N and O elements were displayed in the spectra sur-vey for the two samples and no peak assigned to S species could be found for GCN-T (Fig. 3a). The surface C/N atomic ratio of the GCN-T was 1.18 in a semi-quantitative fashion, while that of GCN-D was 1.51. It indicated that the two samples were carbon-rich and nitrogen-poor in terms of the nominal theoretical value of 0.75 for bulk g-C_3N_4. And GCN-D was more enriched with car-bon yet deficient in nitrogen compared to GCN-T. The C1s spectra in Fig. 3b showed three main peaks, which could be assigned to adventitious carbon species (284.8 eV), C—(N)₃ (286.5 eV) and N—C=N (288.1 eV), respectively [23]. The high-resolution N1s spec-tra could be fitted into four peaks centered at about 398.5 eV, 400.1 eV, 401.2 eV and 404.2 eV, respectively (Fig. 3c) [23,25]. The main signals showed the occurrence of the sp²-bonded N involved in the triazine rings (C—N=C, 398.5 eV) and tertiary nitrogen groups (N—(C)₃, 400.1 eV). The weak peak at 401.2 eV indicated the pres-ence of amino functional groups (C—N—H), originating from the defective condensation of heptazine substructures [25]. Addition-ally, the very weak peak at 404.2 eV was attributed to the charging effects or positive charge localization in the heterocycles [25]. There were three main signals in O1s spectra, which could be assigned to the chemisorbed H_2O (533.5 eV), O—C—N (532.4 eV) and hydroxyl groups (–OH, 531.5 eV), respectively [23]. The contained oxygen (O—C—N) in the samples presumably came from the heating treat-ment in the presence of air. It was still emphasized that no sulfur species ($2p_{3/2}$ = 164.0 eV) were detected on the surface of GCN-T by
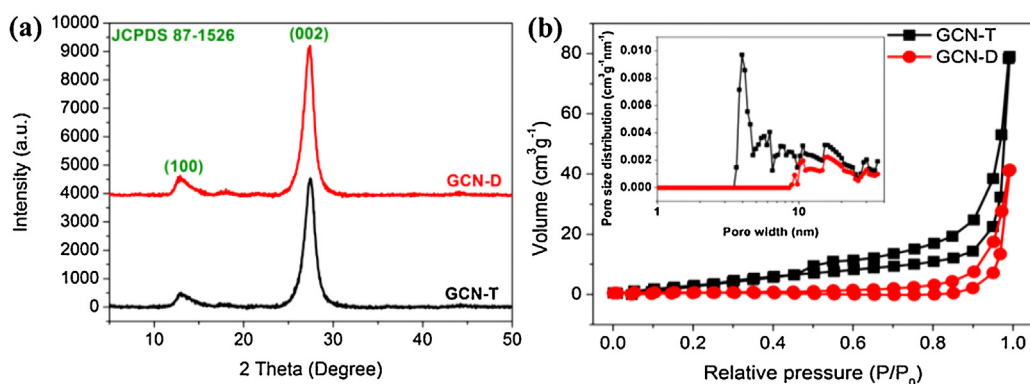

Fig. 1. XRD patterns (a) nitrogen adsorption-desorption isotherms and pore size distribution (b) of GCN-T and GCN-D.
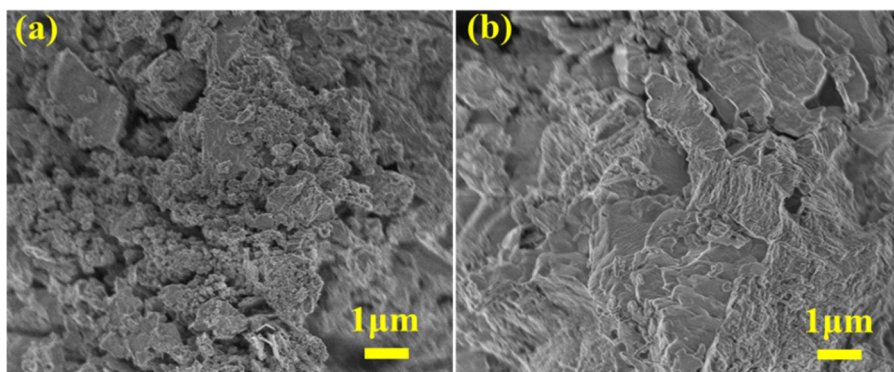

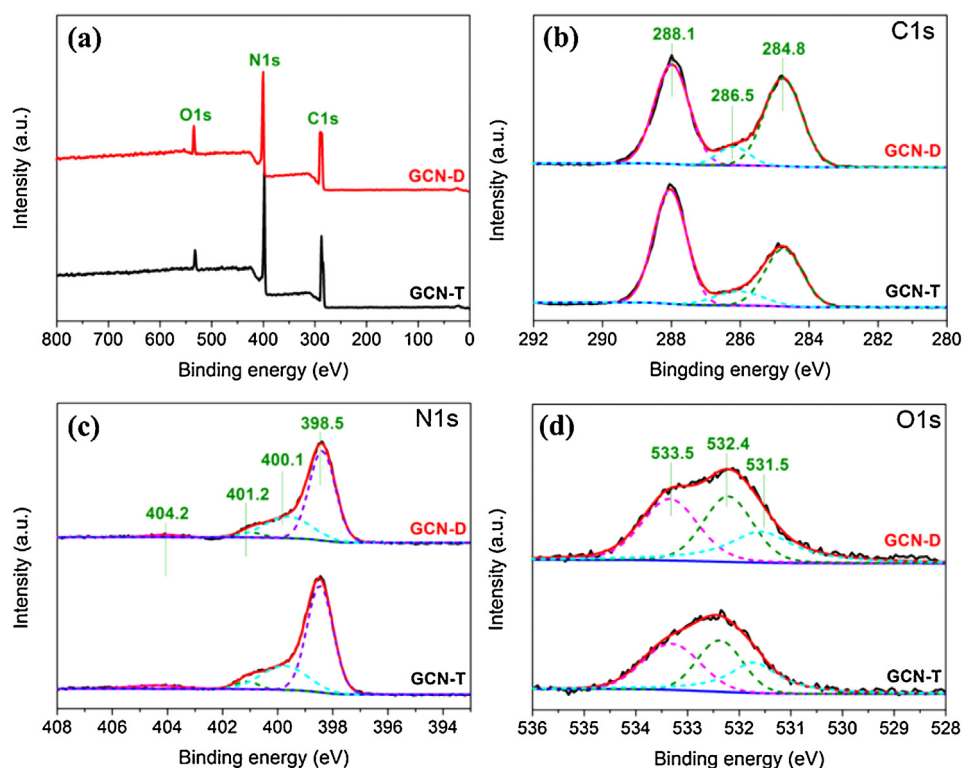**Fig. 2.** FESEM images of GCN-T (a) and GCN-D (b).

Fig. 3. XPS spectra of GCN-T and GCN-D including the survey (a) C1s (b) N1s (c) and O1s (d).
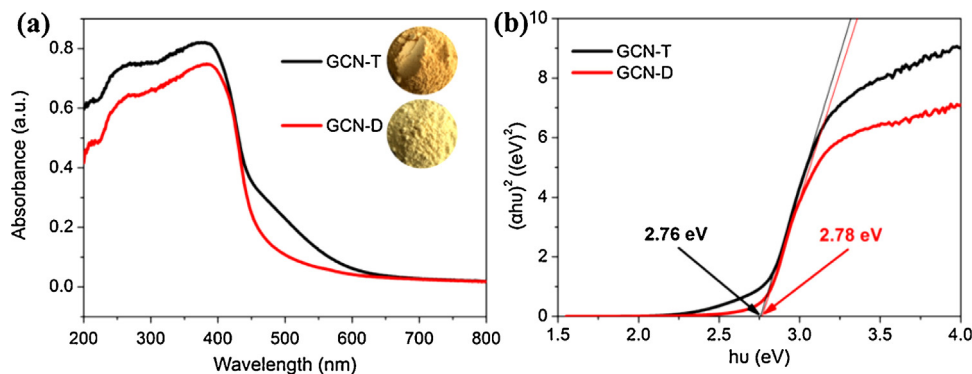

Fig. 4. UV–vis DRS spectra (a) and the bandgaps (b) of GCN-T and GCN-D.

XPS (Fig. S2), which implied that sulfur in thiourea was released into air during the calcination.

3.2. Optical and electronic properties of the photocatalysts

The optical properties of the two samples were examined by UV–Vis DRS, as displayed in Fig. 4a. The bandgaps were determined correspondingly (Fig. 1b). The dark yellow GCN-T showed stronger absorption both in UV and visible-light region compared to the buff-colored GCN-D, mainly due to the different content ratio of C/N and degree of condensation with thiourea and dicyandiamide [23,26]. It was obvious that GCN-T had a shoulder-like improved absorption at between 450 and 600 nm (Fig. 4a), which was in accordance with the reported literatures [23]. The enhanced visible-light absorption of GCN-T was mainly attributed to the enriched nitrogen content compared to GCN-D, leading to the extension of electron delocalization in the aromatic sheets with modified band structure [23,24].

The band gap of GCN-T was 2.76 eV, which was quite close to that of GCN-D (2.78 eV).

Aside from an appropriate bandgap, the matching of CB and VB positions of semiconductor materials with the redox potential of photocatalytic reaction is also important. To determine the relative positions of CB and VB edges, electrochemical Mott–Schottky experiments were performed (Fig. 5a). The positive slope of the plot suggested that GCN-T and GCN-D were n-type semiconductors [27]. The CB position is close to the flat band potential, which can be determined from the intercept on the abscissa [27]. Compared to GCN-T, the CB level of GCN-D was more negative, with a 0.12 V upshift from −0.66 V to −0.78 V vs. SCE at pH 7. Combined with the bandgap values, the VB edges of GCN-T and GCN-D were estimated at 2.10 V and 2.00 V, respectively. The trend of VB (or CB) edge upshift was also evidenced by the VB XPS. The observed VB position upshifted from 2.06 V to 1.99 V (Fig. 5b), while the CB position moved up with a 0.09 V variation from −0.70 V to −0.79 V correspondingly. Fig. 6 shows the energy band structures of the two
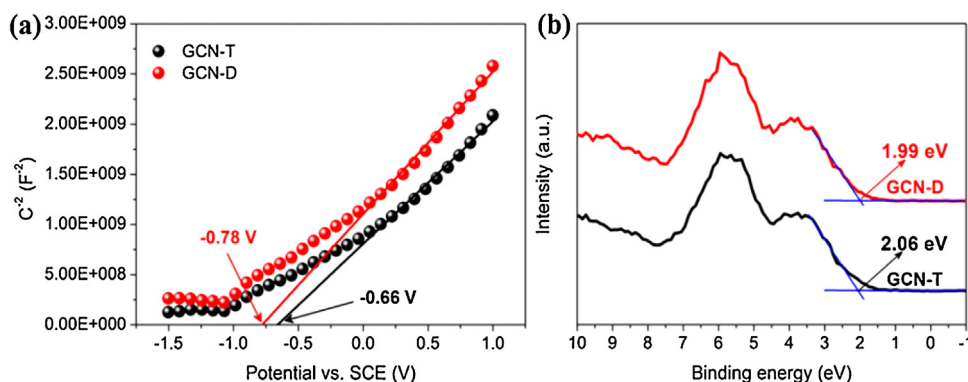
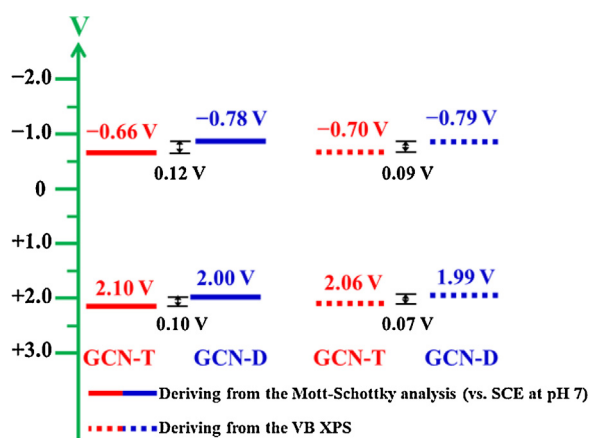**Fig. 5.** Mott–Schottky plots (a) and VB XPS (b) of GCN-T and GCN-D.

Fig. 6. Schematic band structures of GCN-T and GCN-D deriving from the Mott–Schottky analysis and the VB XPS, repectively.

samples, deriving from Mott–Schottky plots and VB XPS, respectively. The upshifted CB (or VB) level of GCN-D was presumably due to its enriched carbon yet low nitrogen content in the g-C_3N_4 crystal in comparison to GCN-T. The more negative CB minimum of GCN-D indicated the generation of stronger reducing electrons under light irradiation. The highly reductive photoexcited electrons should be more easily scavenged by the oxidizing agent, which could promote the charge separation as well as the formation of reactive radicals during photocatalytic reactions.

Furthermore, the electrochemical impedance spectroscopy (EIS) was carried out to gain comprehensive insights into the photogenerated charge separation and transfer process. Fig. 7 shows the EIS Nynquist plots of GCN-T (Fig. 7a) and GCN-D (Fig. 7b) before and after UV or visible-light irradiation, respectively. The arc radius on the EIS Nyquist plot of the GCN-T was smaller than that of GCN-D in the case of UV or visible light irradiation, suggesting that GCN-T owned superior charge distribution and thus made charge transfer easier [8,26]. Interestingly, the charge transfer was improved more under visible light irradiation according to the smaller arc radius on the EIS Nyquist plot compared to that with UV irradiation.

3.3. Photocatalytic ozonation with GCN-T and GCN-D

The photocatalytic ozonation efficiencies of GCN-T and GCN-D were evaluated through the degradation of OA in solution under UV and visible-light irradiation, as shown in Fig. 8c. For comparison, the catalytic ozonation and photocatalytic oxidation of OA were also performed, which are presented in Fig. 8a and b, respectively. The photocatalytic degradation and photocatalytic ozonation of OA generally followed pseudo-zero-order kinetics according to

the linear trends of C/C_0 versus the irradiation time (Fig. 8b and c). And the apparent rate constants were calculated correspondingly, as shown in Fig. 8d and Table 1. It was obvious that GCN-T and GCN-D had negligible activity in catalytic ozonation of OA (Fig. 8a). The photocatalytic degradation of OA was improved when changing visible-light irradiation into high-energy UV illumination (Fig. 8b). Despite all this, the photocatalytic efficiency was still limited with about 20% OA removal at 30 min and a rate constant of 6.70×10^{-3} mM/min in UV/GCN-T system. When combined with ozone, the apparent rate constant of UV/O_3/GCN-D increased to 2.00×10^{-2} mM/min, which was 3.0 times as high as the sum of that in UV/GCN-T and O_3. Notably, the rate constant of OA removal by UV/O_3 was as high as 4.09×10^{-2} mM/min, and the addition of GCN-T or GCN-D moderately inhibited the OA degradation in photocatalytic ozonation with UV irradiation. Under UV with wavelength below 300 nm especially at 254 nm, photolysis of ozone took place and a large amount of reactive atomic oxygen (O (^{1}D)) was generated (Eq. (1)) [16,28]. The O (^{1}D) could quickly convert into •OH and consequently improved oxidation efficiency (Eq. (2)) [16,28].

$$O_3 \xrightarrow{h\nu} O_2 + O(^1D) \tag{1}$$

$$O(^1D) + H_2O \rightarrow H_2O_2 \rightarrow 2 \cdot OH \tag{2}$$

However, when GCN-T or GCN-D was added into the solution, the UV photons were largely captured by the semiconductor materials while the photolysis of ozone was inhibited correspondingly. The photocatalytic reaction pathways were thereby changed and the production of oxidative radicals was presumably decreased in the UV/O_3/GCN-T and UV/O_3/GCN-D systems.

In addition, a super synergistic effect of ozonation and photocatalysis was obviously observed with bulk g-C_3N_4 as the catalyst under visible light, which reconfirmed the finding in our previous work [18]. The highest coupling coefficient was achieved with GCN-D as the catalyst. The Vis/O_3 had negligible efficiency on OA degradation while the apparent rate constant of OA removal by Vis/O_3/GCN-D was 3.30×10^{-2} mM/min, which was 20.6 times as great as the sum of that when OA was treated by Vis/GCN-D and ozonation alone. The GCN-D-triggered coupling coefficient was even higher than that of bulk g-C_3N_4 prepared from melamine (17.8) in our previous work [18]. Aside from OA removal, PHBA was chosen as another representative pollutant to verify the enhanced photocatalytic ozonation efficiency of bulk g-C_3N_4 under visible light. Fig. 9 shows the TOC removal of PHBA as a function of reaction time. During 90 min illumination, the TOC removal by Vis/GCN-T or Vis/GCN-D was only about 3.5%, while that of PHBA was 55.2% for ozonation alone. Vis/O_3 and O_3/g-C_3N_4 had nearly the same mineralization efficiency of PHBA as individual ozonation. At 90 min, about 98.0% and 94.0% of TOC was removed by photo-
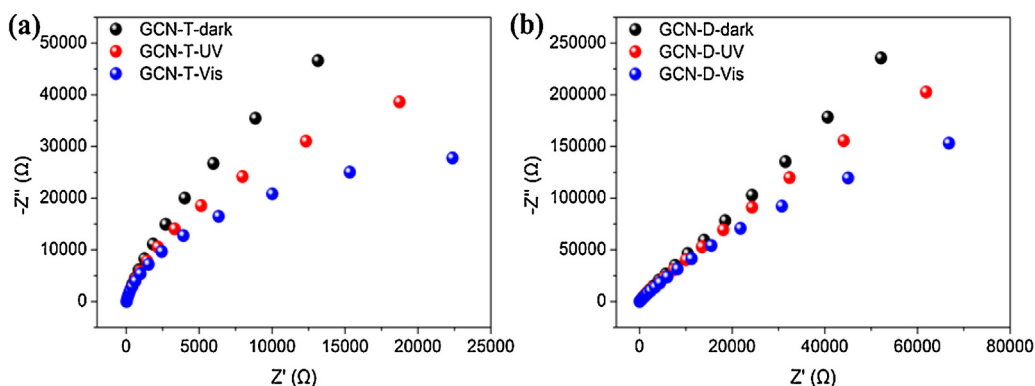
Fig. 7. EIS Nyquist plots of GCN-T (a) and GCN-D (b) with light on/off cycles under the irradiation of UV (200–400 nm) and visible light (420–800 nm).
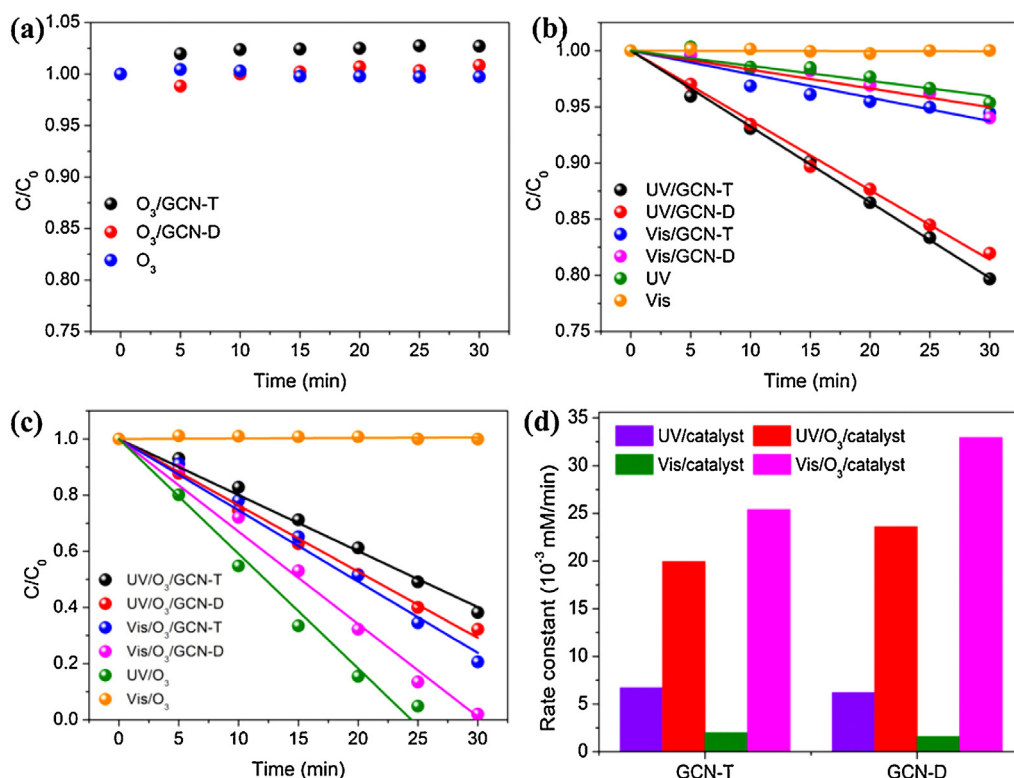

Fig. 8. Degradation of OA by catalytic ozonation (a) photocatalytic oxidation (b) and photocatalytic ozonation (c) with UV or visible light irradiation and the apparent rate constants (d) for OA decomposition by photocatalysis and photocatalytic ozonation with suspension of GCN-T and GCN-D (gas flow rate: 100 mL/min; ozone concentration: 30 mg/L; light intensity: 365 mW/cm^2; initial volume of solution: 300 mL; initial OA concentration: 90 mg/L; catalyst dosage: 1 g/L).

Table 1
Pseudo zero-order rate constants of OA degradation by various oxidation methods.

Catalyst	Rate constant (10^{-3} mM/min)							
	UV/cata.	UV	Vis/cata.	Vis	UV/O$_3$/cata.	UV/O$_3$	Vis/O$_3$/cata.	Vis/O$_3$
GCN-T	6.7	1.34	2	~0	19.95	40.86	25.39	~0
GCN-D	6.2	1.34	1.6	~0	23.61	40.86	32.95	~0

catalytic ozonation with GCN-D and GCN-T, which was 39.3% and 35.3% higher than the sum of that by visible-light photocatalysis and ozonation, respectively.

From the aspect of catalysts, GCN-T exhibited a little higher photocatalytic activity than GCN-D under UV or visible light irradiation (Fig. 8b). The superiority of GCN-T was comprehensible because it had higher surface area, stronger light absorption and faster charge transfer compared to GCN-D. However, the inverse

trend was obtained in photocatalytic ozonation process (Fig. 8c and d). The apparent photocatalytic ozonation rate constants of GCN-D were 3.30×10^{-2} mM/min and 2.36×10^{-2} mM/min under visible light and UV irradiation, which were about 1.30 and 1.18 times as high as that of the GCN-T, respectively (Table 1). Vis/O$_3$/GCN-D also exhibited about 4% higher TOC removal efficiency than Vis/O$_3$/GCN-T in PHBA mineralization (Fig. 9). The enhanced photocatalytic ozonation efficiency of GCN-D was more likely attributed to the
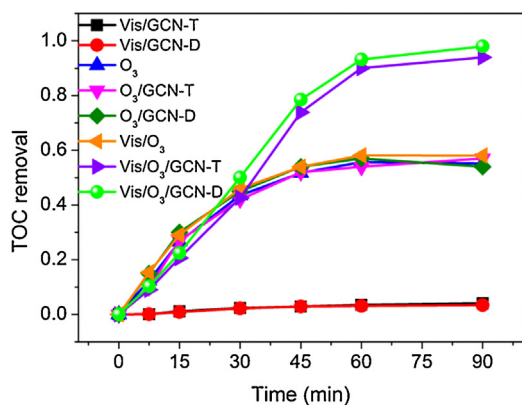
Fig. 9. TOC removal of PHBA degradation by various processes (gas flow rate: 100 mL/min; ozone concentration: 30 mg/L; light intensity: 365 mW/cm^2; initial volume of solution: 400 mL; initial PHBA concentration: 40 mg/L; catalyst dosage: 1 g/L).

upshifted CB level with the generation of more reducing photoinduced electrons. The CB electrons with higher deoxidizing degree could be more easily and quickly captured by the strong oxidizing ozone, which dramatically promote charge separation as well as the decay of ozone decomposition. This result indicated that the CB position was a considerably significant factor in determining the photocatalytic ozonation activity of the semiconductor material. More negative CB potential of the semiconductor material benefited the oxidation ability of photocatalytic ozonation process. Interestingly, Vis/O$_3$/g-C$_3$N$_4$ revealed stronger oxidizing ability in OA degradation than UV/O$_3$/g-C$_3$N$_4$ with the same light intensity (Fig. 8d and Table 1). This fact could be explained by two reasons. One might be that the photolysis of ozone and ozone capturing photoinduced electrons inhibited with each other under UV [16,28]. Thus, a less amount of reactive species were generated in the photocatalytic ozonation process. The other was that the charge transfer turned faster under visible-light irradiation than that with UV irradiation according to the EIS result (Fig. 7), which accelerated the electron capture by ozone under visible light. This result was remarkable for it could contribute to the advance of this energy-saving and environmentally friendly water treatment technology using solar energy.

3.4. Mechanism for enhanced photocatalytic ozonation

The visible-light photocatalytic ozonation of OA with varied ozone concentration was performed to reveal the role of ozone in the combined process, as shown in Fig. 10a and Fig. S3. The photocatalytic ozonation efficiency was significantly enhanced when the concentration of ozone increased from 5 mg/L to 45 mg/L, while further improvement of ozone concentration made a negligible difference. It indicated that the ozone was insufficient for the scavenging of photoinduced electrons when the intrant concentration was below 45 mg/L. An ozone dosage of 4.5 mg/min (100 mL/min of flow rate and 45 mg/L of ozone concentration) could exactly match the generation rate of electrons over the CB of GCN-D. In this situation, the apparent rate constant of OA removal was 4.83 × 10^{-2} mM/min, which was higher than that by UV/O$_3$ with an intrant ozone concentration of 30 mg/L. This indicated that superior photocatalytic ozonation efficiency could be achieved under sunlight instead of artificial UV lamps through the adjustment of some operation parameters like ozone dosage. Ozone here mainly acted as an efficient scavenger for the photoinduced electrons, which could significantly promote the charge separation in photocatalytic reactions. Unlike the common traps such as metal ions, ozone was also a strong oxidant and the combination of ozone and electrons

also contributed to the decay of ozone into reactive radicals. The procedure that ozone captures photogenerated electrons was crucial because it caused electron-hole separation as well as ozone decomposition, which synergistically promoted the generation of more reactive radicals in the solution.

To further reveal the mechanism, the main oxidative species in the photocatalytic degradation and photocatalytic ozonation processes were detected, as shown in Fig. 10b and c. A series of trapping experiments were adopted using N$_2$, tBA and pBQ as the scavengers for reactive oxygen species (ROS), •OH and superoxide radicals (•O$_2^-$), respectively [18,29]. As displayed in Figs. 10 b and S4a, the OA degradation rate constant decreased slightly with the addition of 100 mM of tBA, while that reduced moderately in the presence of 10 mM pBQ. It indicated that •O$_2^-$ played a more significant role than •OH in photocatalytic degradation of OA. The continuous N$_2$ purging completely blocked the OA degradation, suggesting ROS were the dominant oxidative species. Hence, it could be concluded that the photocatalytic degradation was attributed to the direct reaction of OA with ROS including •O$_2^-$ and •OH.

The addition of 100 mM tBA completely inhibited OA degradation in UV/O$_3$ and Vis/O$_3$/GCN-D (Figs. 10 c and S4b). It indicated that •OH was generated and totally responsible for the OA oxidation into water and carbon dioxide in these two processes. However, the generation of •OH in UV/O$_3$ and Vis/O$_3$/GCN-D followed disparate pathways. In UV/O$_3$ system, ozone absorbed some of the incoming photons of UV with wavelength below 300 nm and decomposed into O (^{1}D) (Eq. (1)). It then reacted with water forming H$_2$O$_2$ and subsequently converted into •OH (Eq. (2)). In the Vis/O$_3$/GCN-D system, GCN-D could absorb the visible-light photons to generate electrons upon CB and holes (h$^+$) upon VB (Eq. (3)). The CB potential of GCN-D was as low as −0.78 V (versus SCE at pH 7), which dramatically facilitated CB electron capture by ozone. An ozonide radical (•O$_3^-$) was thus formed (Eq. (4)), and it rapidly reacted with H$^+$ in the solution to give a HO$_3$• radical (Eq. (5)), which subsequently decomposed into •OH (Eq. (6)).

$$GCN\text{-}D \xrightarrow{Vis} e^- + h^+ \tag{3}$$

$$O_3 + e^- \rightarrow \cdot O3^- \tag{4}$$

$$\cdot O_3^- + H^+ \rightarrow HO_3\cdot \tag{5}$$

$$HO_3\cdot \rightarrow O_2 + \cdot OH \tag{6}$$

Notably, h$^+$ were incapable to directly oxidize the surface hydroxyl groups or adsorbed water molecules to form •OH, as the VB potential of g-C$_3$N$_4$ is less than E^0 (•OH/OH$_{suf}^-$) or E^0 (•OH/H$_2$O$_{ads}$) [18,19]. Moreover, the VB of g-C$_3$N$_4$ is reported to be +1.4 V versus NHE [2], while the redox potential of ozone is +2.08 V versus NHE [16]. This means ozone molecular has a higher oxidizing ability than h$^+$. As Fig. 8a shows that ozone could not directly oxidize OA, neither can h$^+$. Hence, h$^+$ was inefficient for the degradation of OA in Vis/g-C$_3$N$_4$ and Vis/O$_3$/g-C$_3$N$_4$. During photocatalytic ozonation, photogenerated electrons would preferentially combine with ozone rather than h$^+$, but h$^+$ in the system may still led to partial combination of electron and hole, and slightly goes against the removal of OA.

In UV/O$_3$/GCN-D process, it was interesting that the OA degradation was significantly suppressed by the addition of tBA but not abolished completely (Figs. 10 c and S4b). •OH was formed in the same manner as that in Vis/O$_3$/GCN-D (Eq. (3)–(6)), which was dominantly responsible for the OA degradation in UV/O$_3$/GCN-D process. Besides that, a small part of OA was presumably oxidized by O (^{1}D) generated through the photolysis of ozone under UV. It implied that a smaller amount of •OH was generated in UV/O$_3$/GCN-D accompanied by a few O (^{1}D). This was the main reason why Vis/O$_3$/GCN-D was more efficient than UV/O$_3$/GCN-D in terms of OA degradation. Based on the above analysis, the degradation mecha-
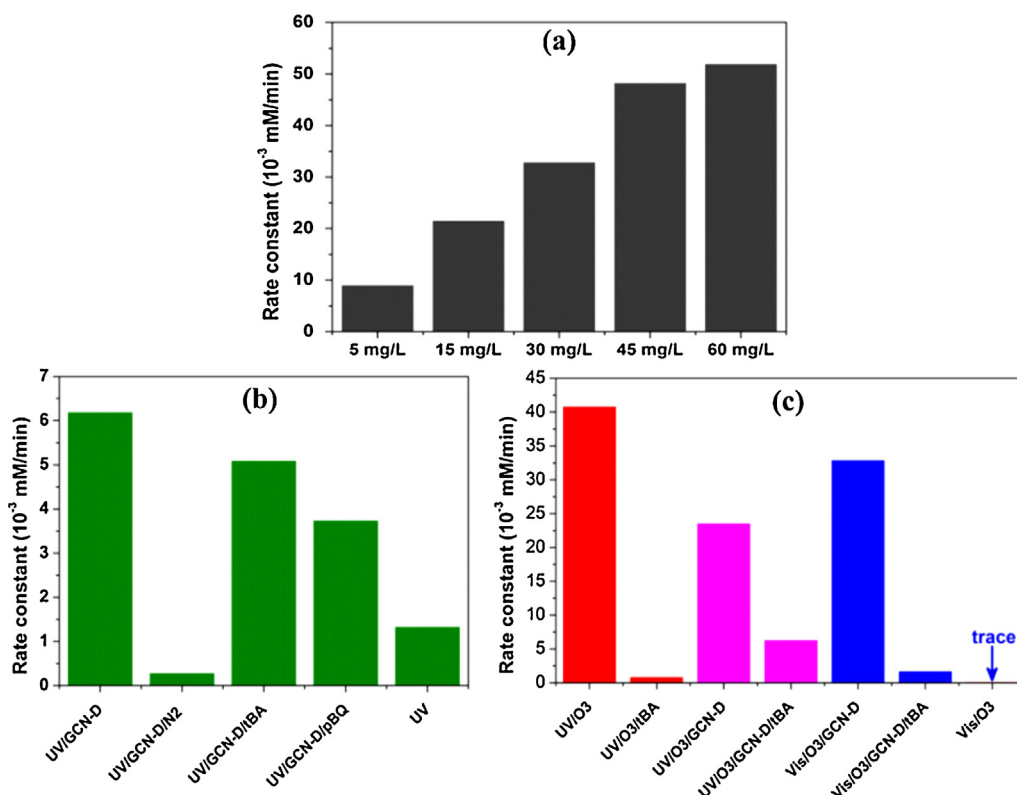
Fig. 10. Influence of intrant ozone concentration on the apparent rate constant of OA removal by Vis/O_3/GCN-D (a) apparent rate constants of OA removal by UV/GCN-D (b) UV/O_3/GCN-D (c) and Vis/O_3/GCN-D (c) in the presence of various scavengers.
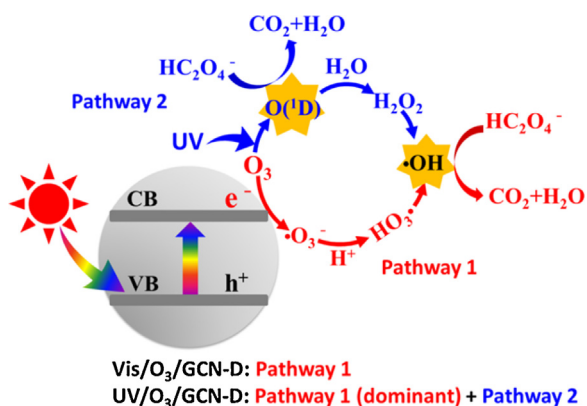

Fig. 11. Schematically illustration of OA degradation by Vis/O_3/GCN-D and UV/O_3/GCN-D processes.

nism for photocatalytic ozoantion of OA under UV and visible-light irradiation was proposed, as illustrated in Fig. 11. •OH was generated from ozone scavenging photoexcited electrons (Pathway 1 in Fig. 11, Eq. (3)–(6)) and completely responsible for OA degradation in Vis/O_3/GCN-D. Besides the dominantly-functioned •OH, a small amount of O (^{1}D) was formed in the UV/O_3/GCN-D system through the photolysis of ozone (Pathway 2 in Fig. 11, Eq. (1)–(2)), which also played a small part for OA degradation by UV/O_3/GCN-D.

4. Conclusion

In summary, bulk g-C_3N_4 exhibited negligible efficiency in catalytic ozonation and limited photocatalytic mineralization of organic pollutants, while it triggered a super synergy between visible-light photocatalysis and ozonation. The apparent rate con-

stant of OA removal by Vis/O_3/GCN-D was 20.6 times as great as the sum of that in Vis/GCN-D and ozonation. The TOC removal of PHBA by Vis/O_3/GCN-D was 39.3% higher than the sum of that in Vis/GCN-D and ozonation. The upshifted CB position was crucial for triggering the synergy, and GCN-D showed 1.3 times higher photocatalytic ozonation activity than GCN-T for its ∼0.10 V upshifted CB level. More negative CB potential benefited the capture of photoinduced electron by ozone molecules, contributing to vigorous charge separation and the decay of ozone. These two aspects synergistically promote the generation of •OH, the only and dominant reactive species in Vis/O_3/GCN-D and UV/O_3/GCN-D, respectively.

Vis/O_3/g-C_3N_4 revealed stronger oxidation ability than UV/O_3/g-C_3N_4 with the same light intensity. It resulted from the photolysis of ozone under UV with wavelength below 300 nm, which partly inhibited ozone capturing the photoinduced electrons. Consequently, the amount of generated •OH decreased in UV/O_3/GCN-D instead with formation of a few O (^{1}D) in comparison to Vis/O_3/GCN-D. This interesting perspective contributes to the potential application of sunlight/O_3/g-C_3N_4 method for water decontamination.

Appendix A. Supplementary data

Supplementary data associated with this article can be found, in the online version, at http://dx.doi.org/10.1016/j.apcatb.2015.08.020

References

[1] Y.J. Cui, J.H. Huang, X.Z. Fu, X.C. Wang, Catal. Sci. Technol. 2 (2012) 1396–1402.
[2] H.Q. Sun, G.L. Zhou, Y.X. Wang, A. Suvorova, S.B. Wang, ACS Appl. Mater. Interfaces 6 (2014) 16745–16754.
[3] H.T. Ren, S.Y. Jia, Y. Wu, S.H. Wu, T.H. Zhang, X. Han, Ind. Eng. Chem. Res. 53 (2014) 17645–17653.
[4] X.J. Bai, L. Wang, Y.J. Wang, W.Q. Yao, Y.F. Zhu, Appl. Catal. B: Environ. 152 (2014) 262–270.
[5] Y. Wang, X.C. Wang, M. Antonietti, Ang. Chem. Int. Ed. 51 (2012) 68–89.
[6] M. Zhang, J. Xu, R.L. Zong, Y.F. Zhu, Appl. Catal. B: Environ. 147 (2014) 229–235.
[7] X.F. Chen, J.S. Zhang, X.Z. Fu, M. Antonietti, X.C. Wang, J. Am. Chem. Soc. 131 (2009) 11658–11659.
[8] M. Zhang, X.J. Bai, D. Liu, J. Wang, Y.F. Zhu, Appl. Catal. B: Environ. 164 (2015) 77–81.
[9] G. Liu, P. Niu, C.H. Sun, S.C. Smith, Z.G. Chen, G.Q. Lu, H.M. Cheng, J. Am. Chem. Soc. 132 (2010) 11642–11648.
[10] L.G. Zhang, X.F. Chen, J. Guan, Y.J. Jiang, T.G. Hou, X.D. Mu, Mater. Res. Bull. 48 (2013) 3485–3491.
[11] S.F. Chen, Y.F. Hu, S.G. Meng, X.L. Fu, Appl. Catal. B: Environ. 150 (2014) 564–573.
[12] Z.A. Huang, Q. Sun, K.L. Lv, Z.H. Zhang, M. Li, B. Li, Appl. Catal. B: Environ. 164 (2015) 420–427.
[13] D.S. Wang, H.T. Sun, Q.Z. Luo, X.L. Yang, R. Yin, Appl. Catal. B: Environ. 156 (2014) 323–330.
[14] L. Ge, C.C. Han, J. Liu, J. Mater. Chem. 22 (2012) 11843–11850.
[15] M. Mehrjouei, S. Müller, D. Möller, Chem. Eng. J. 263 (2015) 209–219.
[16] J.D. Xiao, Y.B. Xie, H.B. Cao, Chemosphere 121 (2015) 1–17.
[17] A. Rey, P. García-Muñoz, M.D. Hernández-Alonso, E. Mena, S. García-Rodríguez, F.J. Beltrán, Appl. Catal. B: Environ. 154 (2014) 274–284.
[18] J.D. Xiao, Y.B. Xie, H.B. Cao, Y.Q. Wang, Z.J. Zhao, Catal. Commun. 66 (2015) 10–14.
[19] G.Z. Liao, D.Y. Zhu, L.S. Li, B.Y. Lan, J. Hazard. Mater. 280 (2014) 531–535.
[20] Z.Q. He, X. Xu, S. Song, L. Xie, J.J. Tu, J.M. Chen, B. Yan, J. Phys. Chem. C 112 (2008) 16431–16437.
[21] H.B. Cao, L.L. Xing, G.G. Wu, Y.B. Xie, S.Y. Shi, Y. Zhang, D. Minakata, J.C. Crittenden, Appl. Catal. B: Environ. 146 (2014) 169–176.
[22] H.H. Ji, F. Chang, X.F. Hu, W. Qin, J.W. Shen, Chem. Eng. J. 218 (2013) 183–190.
[23] F. Dong, Y.J. Sun, L.W. Wu, M. Fu, Z.B. Wu, Catal. Sci. Technol. 2 (2012) 1332–1335.
[24] G.G. Zhang, J.S. Zhang, M.W. Zhang, X.C. Wang, J. Mater. Chem. 22 (2012) 8083–8091.
[25] B.H. Long, J.L. Lin, X.C. Wang, J. Mater. Chem. A 2 (2014) 2942–2951.
[26] F. Dong, Z.W. Zhao, T. Xiong, Z.L. Ni, W.D. Zhang, Y.J. Sun, W.K. Ho, ACS Appl. Mater. Interfaces 5 (2013) 11392–11401.
[27] S. Chu, Y. Wang, Y. Guo, J.Y. Feng, C.C. Wang, W.J. Luo, X.X. Fan, Z.G. Zou, ACS Catal. 3 (2013) 912–919.
[28] Y. Jing, L.L. Li, Q.Y. Zhang, P. Lu, P.H. Liu, X.H. Lü, J. Hazard. Mater. 189 (2011) 40–47.
[29] Z.F. Huang, J.J. Zou, L. Pan, S.B. Wang, X.W. Zhang, L. Wang, Appl. Catal. B: Environ. 147 (2014) 167–174.